横流れ擾乱のPSE解析

野村聡幸（航技研）

PSE analysis of crossflow disturbances

Toshiyuki Nomura*

* National Aerospace Laboratory

Abstract

We have developed a system for prediction of boundary-layer transition. The system consists of a Navier-Stokes code and two codes based on linear parabolized stability equations. The location of the onset of transition is estimated on the basis of the *N* factor. The system is applied to swept-cylinder boundary layers with stationary crossflow disturbances. The wavelength of the disturbance whose *N*-factor curve first reaches 6 agrees approximately with the wavelength observed in the experiment.

Key words: Boundary-layer transition, PSE, swept cylinder, crossflow disturbances

1. Introduction

CFD has been playing an important role in aerodynamic design. However, it is still difficult to precisely estimate friction drag from numerical solutions that a Reynolds-averaged Navier-Stokes code yields. It is because of the accuracy of a turbulence model used and the neglect of laminar-turbulent transition. If it is possible to locate the onset of transition, more accurate friction drag will be obtained by using a turbulence model downstream of the location. A numerical tool coupling with CFD to locate the onset of transition is desirable.

We have developed a system for prediction of boundary-layer transition.[1] The system consists of a Navier-Stokes code[2] and two codes based on linear parabolized stability equations (PSE). The location of the onset of transition is estimated on the basis of the *N* factor. All the equations are formulated in generalized curvilinear coordinates, and all the codes use the same computational grid. Moreover, the PSE are free from the parallel-flow approximation.

Creel, Beckwith, and Chen[3] conducted transition experiments on a swept cylinder at Mach 3.5. In the experiments, stationary crossflow disturbances were observed with oil flow at two Reynolds numbers. The purpose of this paper is to validate the prediction system by capturing the crossflow disturbances.

2. System for prediction of boundary-layer transition

A compressible flow around a body is computed by the Navier-Stokes code, and then a boundary-layer flow is extracted from the converged flow for linear stability analysis. One of the stability analysis codes searches for an initial disturbance, and another conducts space marching of the disturbance. The spatial growth rates of the disturbance are integrated to obtain the *N* factor. The location of the onset of transition is estimated on the basis of the *N* factor.

2.1 Navier-Stokes simulation

A computational grid is generated by Takanashi's method,[4] and then a compressible flow around a body is computed by the Navier-Stokes code. Let ξ, η, ζ, and τ be the surface coordinate in the normal-chord direction, the coordinate normal to the surface, the coordinate in the spanwise direction, and time, $\hat{Q}$ the vector of dependent variables, $\hat{E}$, $\hat{F}$, and $\hat{G}$ the inviscid-flux vectors, $\hat{F}_v$ the viscous-flux vector, and Re the Reynolds number. The thin-layer Navier-Stokes equations that are the governing equations for the Navier-Stokes code can be written as

$$\frac{\partial \hat{Q}}{\partial \tau}+\frac{\partial \hat{E}}{\partial \xi}+\frac{\partial \hat{F}}{\partial \eta}+\frac{\partial \hat{G}}{\partial \zeta}=\frac{1}{Re}\frac{\partial \hat{F}_v}{\partial \eta}, \qquad (2.1)$$

which are numerically solved with a finite-volume method. The inviscid-flux vectors of third-order accuracy

in space are computed by the Chakravarthy-Osher TVD scheme,[5] and the viscous-flux vector of second-order accuracy in space by Gauss' theorem. The diagonalized ADI scheme by Pulliam and Chaussee[6] is used for time integration. A boundary-layer flow is extracted from the converged flow for linear stability analysis.

2.2 Linear stability analysis

An instantaneous flow may be represented as the sum of a mean flow denoted by $\bar{}$ and a disturbance denoted by $\tilde{}$

$$u=\bar{u}+\tilde{u},\ v=\bar{v}+\tilde{v},\ w=\bar{w}+\tilde{w},\\ \rho=\bar{\rho}+\tilde{\rho},\ T=\bar{T}+\tilde{T}, \tag{2.2}$$

where u, v, and w are the velocity components in Cartesian coordinates, ρ the density, and T the temperature. The disturbance in a boundary layer nonparallel to the ξ direction may be written as

$$\tilde{q}(\xi,\eta,\zeta,\tau)=\hat{q}(\xi,\eta)\exp\left[i\left\{\int_{\xi_0}^{\xi}\alpha(\bar{\xi})\,d\bar{\xi}+\beta\zeta-\omega\tau\right\}\right], \tag{2.3}$$

where $\tilde{q}$ is the disturbance vector defined by $(\tilde{u},\tilde{v},\tilde{\rho},\tilde{T},\tilde{w})^T$, $\hat{q}$ the corresponding shape function written as $(\hat{u},\hat{v},\hat{\rho},\hat{T},\hat{w})^T$, and ξ_0 the location of the onset of instability. Here, spatial stability is dealt with. The real wavenumber β and the real frequency ω are known, while the complex wavenumber α is sought.

Substituting equations (2.2) and (2.3) into equation (2.1), subtracting the mean-flow terms, and eliminating the terms including the product of the shape functions yield linear PSE

$$D\hat{q}+A\frac{\partial\hat{q}}{\partial\xi}+B\frac{\partial\hat{q}}{\partial\eta}=V\frac{\partial^2\hat{q}}{\partial\eta^2}, \tag{2.4}$$

where D, A, B, and V are 5×5 matrices. The boundary conditions for equation (2.4) are

$\hat{u}=\hat{v}=\hat{w}=\hat{T}=0$ on the surface $(\eta=0)$,

$\hat{u}$, $\hat{v}$, $\hat{w}$, $\hat{\rho}$, $\hat{T}\to 0$ in the freestream $(\eta\to\infty)$.

In equation (2.4), $\partial\hat{q}/\partial\xi$ is approximated with a first-order backward difference, and $\partial\hat{q}/\partial\eta$ and $\partial^2\hat{q}/\partial\eta^2$ with a second-order central difference. An extension of Malik's global method[7] to spatial stability searches for an initial disturbance, and then a PSE code based on the Bertolotti-Herbert method[8] conducts space marching of the disturbance.

The N factor is defined by

$$N=-\int_{\xi_0}^{\xi}\alpha_i(\bar{\xi})\,d\bar{\xi},$$

where the subscript i denotes an imaginary part. In case of crossflow instability, the N factor for the onset of transition is assumed to be around 6.[9]

3. Results

Creel, Beckwith, and Chen[3] conducted transition experiments on a cylinder of sweep angle of 60° in NASA Langley's Mach 3.5 pilot nozzle. In the experiments, stationary crossflow disturbances of wavelength of 0.04 inch at $\theta=90°$ were observed with oil flow at two Reynolds numbers. θ is the angular distance from the attachment line. The Reynolds numbers based on the freestream and the cylinder diameter D of 1 inch were 0.46×10^6 and 0.92×10^6. As shown in figure 1, we simplify the flow by assuming the swept cylinder to be infinite in the spanwise direction. The subscript ∞ denotes the freestream conditions. The flow at each Reynolds number is computed by the Navier-Stokes code, and then PSE analyses of stationary crossflow disturbances are conducted with their spanwise wavenumbers varied.

3.1 Crossflow disturbances

The wavenumbers are defined by

$$\alpha_r=\frac{2\pi}{\lambda_\xi^*}\Delta\xi^*,\ \beta=\frac{2\pi}{\lambda_\zeta^*}\Delta\zeta^*,$$

where the subscript r denotes a real part, λ_ξ^* and $\Delta\xi^*$ are respectively the dimensional wavelength and grid spacing in the ξ direction, and λ_ζ^* and $\Delta\zeta^*$ in the ζ direction. Both $\Delta\xi^*$ and $\Delta\zeta^*$ on the cylinder surface are constant and equal to 0.0105 inch. Because we consider stationary crossflow disturbances, ω is set equal to 0.

PSE analyses are conducted in case of $\beta=-1.15$, -0.859, -0.687, -0.573, and -0.491 at $Re_{\infty,D}=0.46\times10^6$. Figures 2 (a), (b), and (c) show the curves of α_r, $-\alpha_i$, and the N factor respectively. Here, j is the index in the ξ direction, and $j=250$ and 325 correspond to $\theta=0°$ and 90.3° respectively. Each $-\alpha_i$ curve shows transient around the initial point. It is because the effect of boundary-layer nonparallelism is not taken into account in the global method. The N-factor curve of $\beta=-0.859$ first reaches 6, and the N factor is 6.02 at $j=311$ ($\theta=73.4°$). In the experiments, thermocouples were attached to the inside cylinder

surface at $\theta = 0°$, $32.1°$, $39.8°$, and $50.4°$. Transition was not detected at $\theta \leq 50.4°$. We obtain the wavelength of 0.0491 inch at $\theta = 90.3°$ in case of $\beta = -0.859$. The wavelength obtained is almost in agreement with that observed.

PSE analyses are conducted in case of $\beta = -1.72$, -1.15, -0.859, -0.687, -0.573, and -0.491 at $Re_{\infty,D} = 0.92 \times 10^6$. Figures 3 (a), (b), and (c) show the curves of α_r, $-\alpha_i$, and the N factor respectively. The N-factor curve of $\beta = -0.859$ first reaches 6, and the N factor is 6.10 at $j = 292$ ($\theta = 50.6°$). In the experiment, however, transition occurred at $\theta = 0°$ because of spanwise contamination. The wavelength of 0.0489 inch is obtained at $\theta = 90.3°$ in case of $\beta = -0.859$ and agrees approximately with the wavelength observed.

4. Conclusions

Transition experiments on a swept cylinder were conducted at Mach 3.5. In the experiments, stationary crossflow disturbances were observed at two Reynolds numbers. The flow at each Reynolds number is computed by the Navier-Stokes code, and then PSE analyses of stationary crossflow disturbances are conducted with their spanwise wavenumbers varied. At both the Reynolds numbers, the wavelength of the disturbance whose N-factor curve first reaches 6 is almost in agreement with the wavelength observed. However, the relation between the N factor and the transition-onset location is not investigated, because the location was not found in the experiments.

References

[1] Nomura, T. Development of a system for prediction of boundary-layer transition. NAL TR-1397T, 2000.

[2] Nomura, T. Navier-Stokes simulation and linear stability analysis for a boundary layer on the swept cylinder. NAL TR-1321, 1997 (in Japanese).

[3] Creel, T. R., Beckwith, I. E., and Chen, F.-J. Effects of wind-tunnel noise on swept cylinder transition at Mach 3.5. AIAA Paper 86-1085, 1986.

[4] Takanashi, S. and Takemoto, M. A method of generating structured-grids for complex geometries and its application to the Navier-Stokes simulation. CFD J., Vol. 2, No. 2, pp. 209–218, 1993.

[5] Chakravarthy, S. R. Development of upwind schemes for the Euler equations. NASA CR-4043, 1987.

[6] Pulliam, T. H. and Chaussee, D. S. A diagonal form of an implicit approximate-factorization algorithm. J. Comput. Phys., Vol. 39, pp. 347–363, 1981.

[7] Malik, M. R. Finite-difference solution of the compressible stability eigenvalue problem. NASA CR-3584, 1982.

[8] Bertolotti, F. P., Herbert, Th., and Spalart, P. R. Linear and nonlinear stability of the Blasius boundary layer. J. Fluid Mech., Vol. 242, pp. 441–474, 1992.

[9] Arnal, D. Boundary layer transition: predictions based on linear theory. AGARD Report 793, pp. 2/1–63, 1994.

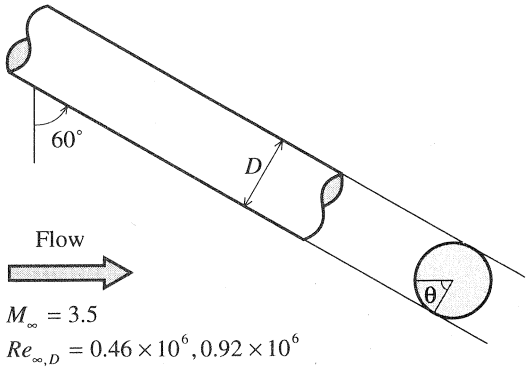

Figure 1: Infinite swept cylinder.

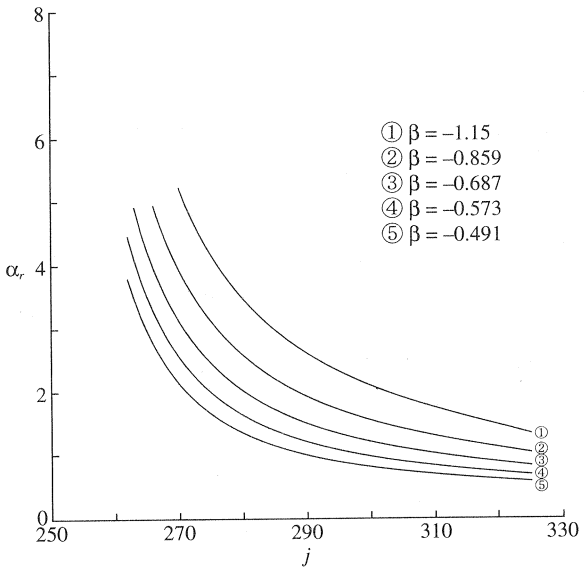

(a) Wavenumbers in the ξ direction.

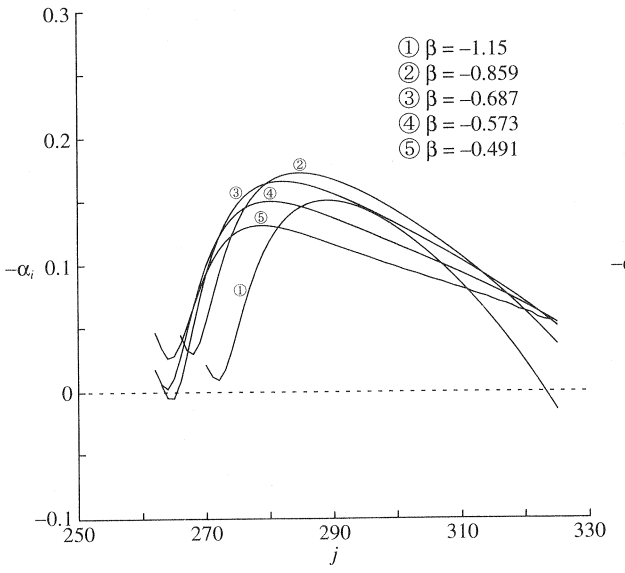

(b) Spatial growth rates in the ξ direction.

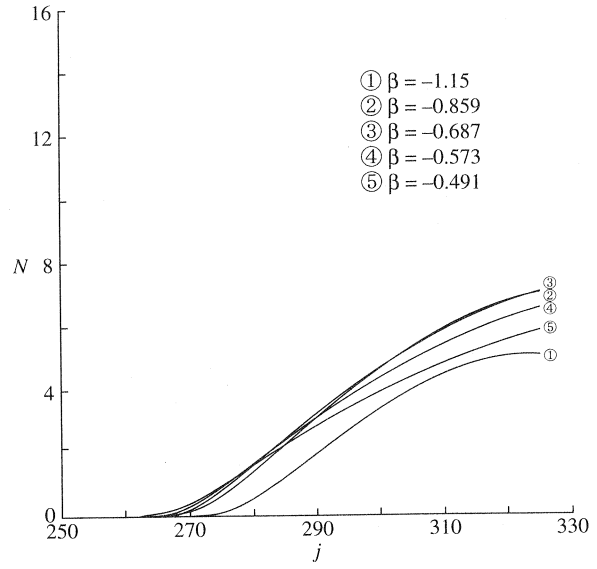

(c) N factors.

Figure 2: PSE solutions at $Re_{\infty,D} = 0.46\times10^6$.

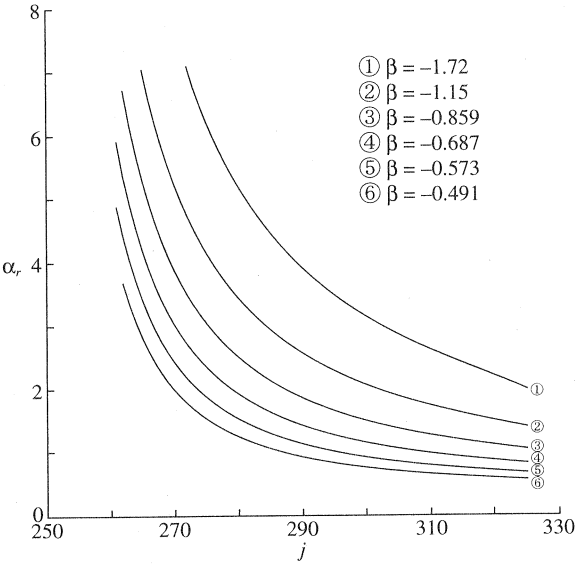

(a) Wavenumbers in the ξ direction.

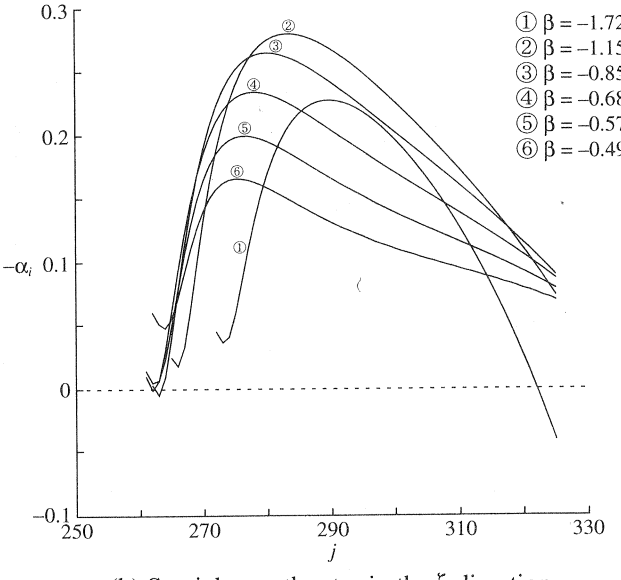

(b) Spatial growth rates in the ξ direction.

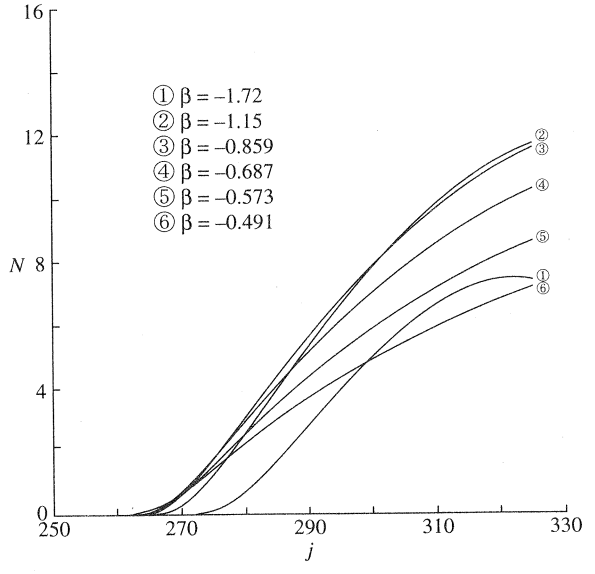

(c) N factors.

Figure 3: PSE solutions at $Re_{\infty,D} = 0.92\times10^6$.